



**HAL**  
open science

# A fuzzy classification of the hydrodynamic forcings of the Rhone River plume: an application in case of accidental release of radionuclides

Adrien Delaval, Celine Duffa, I. Pairaud, Olivier Radakovitch

## ► To cite this version:

Adrien Delaval, Celine Duffa, I. Pairaud, Olivier Radakovitch. A fuzzy classification of the hydrodynamic forcings of the Rhone River plume: an application in case of accidental release of radionuclides. *Environmental Modelling and Software*, 2021, 140, pp.105005. 10.1016/j.envsoft.2021.105005 . hal-03600843v2

**HAL Id: hal-03600843**

**<https://hal.science/hal-03600843v2>**

Submitted on 15 Feb 2023

**HAL** is a multi-disciplinary open access archive for the deposit and dissemination of scientific research documents, whether they are published or not. The documents may come from teaching and research institutions in France or abroad, or from public or private research centers.

L'archive ouverte pluridisciplinaire **HAL**, est destinée au dépôt et à la diffusion de documents scientifiques de niveau recherche, publiés ou non, émanant des établissements d'enseignement et de recherche français ou étrangers, des laboratoires publics ou privés.



Distributed under a Creative Commons Attribution - NonCommercial - NoDerivatives 4.0 International License

# A fuzzy classification of the hydrodynamic forcings of the Rhone River plume: an application in case of accidental release of radionuclides

[Environmental Modelling & Software](#)

DELAVAL<sup>1</sup> A., DUFFA<sup>1</sup> C., PAIRAUD<sup>2,3</sup> I., RADAKOVITCH O.<sup>1,4</sup>

1 - IRSN (Institut de Radioprotection et de Sûreté Nucléaire), PSE-ENV/SRTE/LRTA, 13115 Saint-Paul-Les-Durance, France.

2- UMR 6523 CNRS, IFREMER, IRD, UBO, Laboratoire d'Océanographie Physique et Spatiale, 29280 Plouzané, France

3- IFREMER, Centre Méditerranée, Laboratoire Environnement Ressources Provence Azur Corse, F-83507 La Seyne sur Mer, France

4 - Aix Marseille Univ, CNRS, IRD, INRAE, Coll France, CEREGE, Aix-en-Provence, France

## Abstract

Assessing and modelling the coastal plume dispersion of nuclearized rivers is strategic in case of accidental releases for the protection of vulnerable areas, but taking into account all the possible hydrodynamical conditions is challenging. River plumes are mostly affected by wind and river discharge, but the variability of these two forcings suggest that data mining methods may be particularly effective to define their major trends and influences on the plume behavior.

This study uses fuzzy c-mean clustering on Rhone River (France) discharge and wind speed at its estuary for two objectives: explaining the variability of the riverplume by defining scenarios of hydrodynamic forcings, and relating these scenarios with the

26 spatial extension of the plume . The application to the Rhone River, the most  
27 nuclearized European river, highlighted the ability of this method to classify a 10 years  
28 serie of wind and discharge into 6 scenarios with remarkable characteristics. These  
29 scenarios correspond to different surface currents and plume behaviors, and they were  
30 used to simulate the extension and dilution of a radioactive release. These simulations  
31 can be used as a quick decision tool, and a decisional tree is also proposed to identify in  
32 real time which climatological scenario occurs at the river mouth and the potential  
33 plume pattern.

34 **Keywords :**

35 Coastal plume, Fuzzy c-mean clustering, modelling scenarios, Rhone River, radioprotection, coastal  
36 management

37

38 **1.Introduction :**

39

40 The Rhone River catchment extends over 98000 km<sup>2</sup> and covers one fifth of the French  
41 metropolitan territory. It is the main source of particles and freshwater for the Gulf of  
42 Lion in the North Western Mediterranean sea (Durrieu De Madron et al., 2000), and all  
43 together one of the most important input to the Mediterranean sea (Ludwig et al., 2009).

44 The Rhone valley also hosts the largest concentration of nuclear power plants in Europe  
45 with 4 nuclear power plants in process and a spent fuel reprocessing center, under  
46 dismantlement since 1997. Eyrolle et al. (2020) recently synthesized the studies showing  
47 that this river carries artificial radionuclides from decades, resulting from authorized  
48 releases of low level radioactive liquid wastes and from the export of atmospheric  
49 deposits on watersheds consequently to nuclear weapons testing and Chernobyl accident.

50 France is presently ranked second in the world for the production of nuclear energy, and

51 the total electricity production in the combined regions of Northern, Western and

52 Southern Europe is projected to increase by 2050 (IAEA 2019). Also, the risk of incident

53 on any kind of nuclear installations is still of concern in France and must be taken into  
54 account. As for any river, the transport of artificial radionuclides in case of accidental  
55 release will occur both in dissolved and particulate form, depending on the amount of  
56 suspended particulate matter and on the chemical properties of the radionuclides, and  
57 particularly their distribution coefficient (Tomczak et al., 2019). For the Rhone River, the  
58 prediction of dissolved vs particulate fluxes and the associated time scale for transit can  
59 be evaluated through numerical modeling (Launay et al., 2019), but the behavior of  
60 radionuclides once at sea is clearly less constrained, because it will primarily depend on  
61 the forcings governing the shape of the Rhone River plume.

62 The area of the Rhone river mouth is characterized by a very small tidal amplitude  
63 about 30 cm inducing the formation of a sedimentary delta. As usual in this case, the  
64 freshwater input forms a thin stratified plume of low salinity water (and higher  
65 turbidity) overlying the seawater and extending between 4 and 1000 km<sup>2</sup> (Estournel et  
66 al., 1997; Gangloff et al., 2017) with a thickness decreasing seaward (Pairaud et al.,  
67 2011; Gangloff et al., 2017). It is preferentially deflected westward in a clockwise  
68 orientation running East to West (Reffray et al., 2004) due to the general circulation  
69 induced by the Northern Current along the continental slope. Under north-northwest  
70 winds, the plume extends offshore towards the southwest, whereas it is pushed to the  
71 coast west of the river inlet in case of southeastern winds. Satellite and modelling  
72 results have also shown that the plume size increases with river discharge (Frayse et  
73 al., 2014; Gangloff et al., 2017). More episodic processes impact the plume pattern such  
74 as dense water formation and cascading (Ulses et al., 2008), upwelling cells and marine  
75 storms (Millot, 1990; Millot, 1999). As a result, this plume extends far beyond the coastal  
76 areas and may covers a large area in the GoL extending from the vicinity of the mouth  
77 up to the Cap de Creus at the french-spanish border (Sanchez-Cabeza et al., 1992). It can  
78 also reach the Gulf of Fos (Gontier et al., 1992; Charmasson et al., 1999) or the Bay of

79 Marseille (Pairaud et al., 2011 ; Fraysse et al., 2014) on the eastern side of river mouth.  
80 The Gulf of Fos is an important economic area with one of the biggest commercial port in  
81 Europe and a large shellfish area, and Marseille is one of the biggest Mediterranean  
82 coastal city with one million inhabitants. Due to the oligotrophic nature of the  
83 Mediterranean Sea, the region of freshwater influence (ROFI) of the Rhone river has a  
84 major influence on the distribution of plankton groups (Diaz et al., 2019) and thus  
85 pelagic catches on the GoL. Obviously, the inputs of chemical contaminants from the  
86 Rhone River can greatly affect the fishery activity.

87 The combination of meteorological and hydrodynamic forcings with the dynamics of the  
88 Rhone River discharge results in a large spatio-temporal variability in freshwater and  
89 associated pollutants delivery to the GoL (Martin et al., 2019). If an accidental release  
90 occurs in the Rhone River, the dissolved radionuclides may reach the estuary within 48h  
91 hours to few days depending on the source location and water discharge [unpublished  
92 results]. Once at sea, the different shapes that the plume may present will depend on  
93 hydrodynamic and weather conditions and will lead to contaminate different areas.  
94 Since one goal of radioprotection is to predict the transfer of radionuclides in the  
95 environment, there is a need to anticipate their dispersion at any time and in any kind of  
96 meteorological and hydrodynamical conditions.

97 Different numerical hydrodynamic models have been set up in the GoL, including the  
98 river mouth (Pairaud et al., 2011 ;Duffa et al., 2016), and they could be used actually in  
99 case of accidental release in order to predict the behavior of the freshwater input.  
100 However, the delay necessary for their implementation will range from few hours to few  
101 days, whereas very quick and concise information should be provided to experts and  
102 decision-makers as a first picture of the local issues. Also the potentially impacted zones  
103 will be better defined by performing a fine spatial scale simulation adequately centered ,  
104 compared to a large-scale simulation

105 As a result, a preliminary study embraces all possible plume patterns is necessary, and a  
106 first step is to target the general behavior of the estuarine-plume system. Bárcena et al.,  
107 (2015) explained that two approaches may be conducted for that: simulating several  
108 scenarios using constant conditions of hydrodynamic forcings or simulating few scenarios  
109 using the most frequent or extreme real hydrodynamic forcings during short-medium  
110 term periods (month to year).

111 These authors demonstrated that the first approach is not complete because real forcings  
112 cannot be deduced from the combination of simple idealized scenarios. The second  
113 approach relies on a subjective selection of scenarios by an expert and it will have an  
114 expensive computational cost for simulations if the need is to get an overview of the  
115 different kind of realistic responses of the estuarine-plume mean behavior. In this case,  
116 and to minimize subjectivity, a methodology based on data mining should be able to  
117 select the most relevant condensed hydrodynamic scenarios, taking into account the time  
118 evolution and the occurrence probability of the forcings.

119 Plume classifications based on satellite observations or hydrodynamic model output have  
120 been defined in several river-sea systems using Empirical Orthogonal Function or Self-  
121 Organizing-Map (Falcieri et al., 2014; Xu et al., 2019). Such classification method deals  
122 with large spatial scale but implies a heavy data pretreatment like « masking » to treat  
123 the satellite data or for the computation of the model. In addition, the need of long-term  
124 environmental databases (e.g., 10–20 years) to assess probabilities implies significant  
125 computational costs as well as long and multiple series of data to be used as boundary  
126 conditions and climatic forcings. Another approach is to classify the main hydrodynamics  
127 drivers by looking for example at the catchment discharge and the winds intensities and  
128 directions (Kaufmann & Whiteman 1999; Zhang et al., 2011). Since the plume response  
129 to these forcings can be longer than 24h (Demarcq & Wald, 1984 ; Estournel et al., 1997),  
130 the classification should work observation by observation but must also keep consistency

131 over longer temporal scales of few days in order to be accurate. Clustering performed on  
132 temporal series helps to assess the consistency of a trend over time, and a fuzzy  
133 clustering algorithm provides a continuous cluster membership function allowing to spot  
134 significant trend changes.

135 In this context, this paper presents a methodology based on statistical analysis and  
136 numerical modelling that was developed to address the limitations of the previously  
137 mentioned approaches. Firstly, we used a fuzzy c-mean algorithm to identify and classify  
138 combinations of winds and discharge at the mouth of the Rhone river in order to define  
139 “model scenarios” of realistic forcings. Secondly, the consequences for sea surface  
140 currents will be assessed and the resulting plume pattern will be modeled for each  
141 scenario, as well as the distribution of dissolved radionuclides due to a hypothetical and  
142 episodic release on the Rhone River. These *plumes scenario* can be used as a support for  
143 operational tools improvement and decision.

144

## 145 2. Matériel and Methods

### 146 2.1 Field study and data

147

148 The Rhone River hourly discharges have been provided by the C.N.R (Compagnie  
149 Nationale du Rhône) thanks to the Rhone Sediment Observatory (OSR program). They  
150 were measured at the SORA station, in the city of Arles located 47 km upstream of  
151 Rhone River mouth (Fig 1). It must be noted that the Rhone River splits in two branches  
152 upstream of this station: the Grand Rhone and Petit Rhone. The station reports the  
153 discharge for the Grand Rhone River only, which represents about 90 % of the total  
154 Rhone River discharge (Boudet et al., 2017). In our case we focus only on the river plume  
155 at the Grand Rhone outlet.

156 Weather data and subsurface marine currents data are issued from the MesuRho station  
157 (Pairaud et al., 2016), operational since June 2009 and located at the Buoy Float  
158 Immersed (BFI) maritime buoyage Roustan East (43 ° 19.2 N, 4 ° 52 E) on the Rhone  
159 prodelta (20 m water depth). It is about 1 mile southeast of the mouth and was  
160 configured to collect physico-chemical data in near real time and at high frequency  
161 (about 30 min) in the fresh/marine waters transition zone. It is equipped with a weather  
162 station at 10 m height and an Acoustic Current Doppler Profiler (ADCP). The  
163 instrumentation is connected by a cable to a controller located above the sea surface and  
164 powered by solar panels. The measurements are transmitted to the Coriolis data center  
165 via GPRS (about 1 transmission every 12h since 2015, 4h before).

166 Weather variables used are the average wind speed over 30 min and the gust wind  
167 speed. Gust wind speed is the maximal mean wind speed over 0.5 second observed  
168 during a period of 30 min.

169 The observations used were registered between 2009 and 2019 and result in a total of  
170 128262 data. The subsurface currents (maximum depth of 1.5 m) from 2010 to 2019 were  
171 also used, when available and after quality control validation, leading to a total of 31826  
172 observations.

173 In order to perform multivariate analysis and regression, wind and currents variables  
174 (expressed in terms of velocities  $u$  and directions  $\theta$ ) are described by an Eastward and a  
175 Northward component  $X$  and  $Y$  and calculated as follow :

$$176 \quad \begin{cases} X = u \cdot \cos(\theta) \\ Y = u \cdot \sin(\theta) \end{cases} \quad (1)$$

177 The corresponding hourly discharges in Arles (64131 obs.) were shifted with a 24 h  
178 delay, which corresponds to the transit time between Arles and the river mouth for a  
179 mean liquid discharge.

180

## 181 2.2 Principal Component Analysis

182

183 Principal Component Analysis (PCA) has been widely used in environmental sciences  
184 including hydrologic and hydrodynamics (e.g. Hannah et al., 2000; Paireaud et al., 2008).  
185 The common goal to all principal component methods is to describe a data set ( $X$  with  $i$   
186 individuals or observations and  $w$  variables) using a small number ( $p < w$ ) of uncorrelated  
187 variables, while retaining as much information (variance) as possible. The reduction is  
188 achieved by transforming the data into a new set of continuous variables named the  
189 principal components.

190 The reduction of dimensionality provides a framework to visualize data which is  
191 especially important for large datasets (Husson et al., 2010). This facilitates the analyses  
192 based on geometrical criteria such as separate observations into  $k$  distinct sub-groups  
193 (clustering) or determination of extreme points (Renner, 1993; Napoleon & Pavalakodi,  
194 2011)).

195 Using PCA as a pre-processing tool in order to cluster presents two additional  
196 advantages. The reduction of dimensionality speeds up the convergence of classification  
197 algorithms, which usually depends on the square of  $p$  and  $i$  (Ben-Dor et al., 2004), and it  
198 reduces the noise, the essential of the information being on the first components whereas  
199 the noise is on the lasting ones (Husson et al., 2010). PCA has been performed using the  
200 R package “FactoMineR” (Lê et al., 2008).

## 201 2.3 Fuzzy c-mean algorithm

202 Clustering is a usual method for data mining when it comes to identify groups and  
203 classify individuals, but many algorithms exist and present different results and  
204 convergence speeds (Jain et al., 1999). The first goal is to find an algorithm based on  
205 geometrical criteria as simple as possible for a more realistic interpretability, and the

206 second one is to find a fast convergence algorithm in order to treat the important  
207 dataset.

208 The most usual method is the c-mean or k-mean (MacQueen, 1965 ;Yadav & Sharma,  
209 2013) and its fuzzy alternative (Bezdek, 1981 ; Fu Lai & Tong, 1994). C-means are  
210 iterative algorithms that classify individuals of a dataset into C groups. The algorithm  
211 allows to randomly define C centroids in the same coordinate systems as the individuals.  
212 Each individual x (total of K) is then assigned to the closest centroid center  $c_i$ . The  
213 barycenter of each subgroup is then calculated and becomes the new centroid. Again,  
214 individuals are reassigned to the closest centroid. This iterative procedure minimizes the  
215 objective function (J) and the procedure ends when J reaches an inferior threshold in Eq  
216 (2).

217

$$218 \quad J = \sum_{i=1}^C \sum_{X_k \in C_i} \|x_k - c_i\|^2 \quad (2)$$

219 This method is defined as “crisp”, which means that each observation is set to belong to  
220 its closest centroid cluster. Consequences are that observations with different distances  
221 from the nearest cluster are classified into this cluster without degree of uncertainty and  
222 the ambiguity of the data is eliminated.

223 Cluster boundaries are usually not sharp in environmental sciences (Zadeh et al., 1965),  
224 especially when ambiguous data exist, and membership degrees are more realistic than  
225 crisp assignments (Klawonn & Höppner, 2003). A priori we do not expect a crisp  
226 classification and it is important to have feedback on the confidence of classification for  
227 each individual. As a result, the ambiguity of the data can be preserved and his  
228 probability can be used later for post treatments (Kim et al., 2011).

229 The fuzzy alternative introduces two new parameters. The first one is the membership  
230 coefficient  $\mu_{ik}$ , the coefficient of the  $k$ th observation to the  $i$ th cluster. This membership

231 represents how closely the  $k$ th data object ( $x_k$ ) is located from the  $i$ th cluster center. It  
 232 varies from 0 to 1 depending on the distance ( $\|x_k - c_i\|^2$ ), and a higher membership  
 233 coefficient indicates stronger association between the  $k$ th data object to the  $i$ th cluster.

$$234 \quad \mu_{ik} = \left[ \sum_{j=1}^C \left( \frac{\|x_k - c_i\|^2}{\|x_k - c_j\|^2} \right)^{\frac{2}{m-1}} \right]^{-1} \quad (3)$$

235 The second parameter  $m$  is the fuzziness coefficient. It is greater than 1 and usually  
 236 dependent on the dataset structure because it represents the degree of overlap of the  
 237 clusters (Klawonn & Höppner, 2003). If we set  $m$  to a smaller value, more (less) weight is  
 238 given to the objects that are located closer to (farther from) a cluster center. As  $m$  is close  
 239 to 1,  $\mu_{ik}$  converges to 0 for the objects that are far from a cluster center, or 1 for those  
 240 close to a cluster center, which implies less fuzziness (i.e. clearer cut).

241 The symbol  $\| \cdot \|$  denotes any vector norm that represents the distance between the data  
 242 object and the cluster center. Here we use the 2-norm (Euclidean norm) which is widely  
 243 used in the FCM.

244 The new  $c$ -mean function to minimize becomes:

$$245 \quad J = \sum_{i=1}^C \sum_{k=1}^K (\mu_{ik})^m \|x_k - c_i\|^2 \quad (4)$$

246 The robustness brought by the fuzzy approach over the crisp classification is a  
 247 significant improvement in term of efficiency and convergence. Because each individual  
 248 (observations) has a probability to belong to each center, centers are adjusted faster and  
 249 the algorithm converges faster (Fu Lai & Tong, 1994; Ferraro & Giordani, 2015).

250 Also, without any prior information on the cluster structure (sphericity of clusters,  
 251 possible overlap) the fuzzy  $c$ -mean provides better results than its crisp counterpart  
 252 (Selim & Kamel, 1992). As a result, hydrologic and climatologic combinations can be  
 253 identified by fuzzy  $c$ -mean (Kim et al., 2011; Zhang et al., 2011; Bárcena et al., 2015).

254 In this study the fuzzy-cmean algorithm is performed using the “e1071” package from R  
255 software (Hornik et al., 2019).

256

#### 257 2.4 Choice of the number of clusters $C$ and the coefficient of fuzziness $m$

258 Fuzzy  $c$ -mean algorithm needs to be initialized with the number of clusters  $C$  and the  
259 coefficient of fuzziness  $m$ . The best combination of these parameters is not determined by  
260 the algorithm. One approach is to run different simulations with different  $\{C, m\}$  pairs  
261 and to check the efficiency of clustering with a quality criteria (Ramze Rezaee et al.,  
262 1998; Setnes & Babuška, 1999)

263 Many criteria and their efficiency are available in Wang & Zhang (2007) and Liu et al.  
264 (2010). Some have fast calculation like partition coefficient (PC) or partition entropy  
265 (PE), but they monotonously decrease with the number of clusters and the lack of direct  
266 connection to the geometry of the dataset. Others are more complete but computationally  
267 expensive, such as the Dunn index (Dunn, 1974) or the fuzzy silhouette (Campello &  
268 Hruschka, 2006), and they could not be calculated with this dataset. The Xie and Beni  
269 index (Xie & Beni, 1991) could be calculated based on Eq (5). XB has a direct connection  
270 to the geometrical property of dataset because it takes into account both compacity and  
271 separation of the clusters. It deals correctly with noisy datasets, size or density  
272 variations (Liu et al., 2010).

$$273 \quad XB = \frac{\sum_{i=1}^C \sum_{k=1}^K \mu_{ik}^m \|x_k - c_i\|^2}{K \min_{i,j} \|c_j - c_i\|^2} \quad (5)$$

274 Calculation of XB is also fast for our dataset: from 4 to 10 seconds depending on  $\{C, m\}$   
275 pair.

276  $C$  could be any integer number between 2 and 358, the last one being theoretically the  
277 square root of the dataset length (Chaimontree et al., 2010). The fuzzifier  $m$  can be in

278 theory any real number between 1 and  $\infty$ . In our case, the interval of  $\{C, m\}$  simulations  
279 has been restrained based on the following:

280 - Depending on the river-sea system involved, a different number of plume  
281 patterns exist. In literature, we found that a river plume can present up to 8 patterns  
282 (Xu et al. 2019). As a result, we do not expect our number of cluster to exceed 8 and the  
283 number of clusters  $C$  was set between 2 and 8.

284 - Previous studies report that values of  $m$  can range from 1 to 4. Most of them use  
285  $m \in [1.5, 2.5]$  and as result  $m$  is usually set to 2 by default (Hathaway and Bezdek 2001;  
286 Klawonn & Höppner, 2003). Overall  $m$  is lower for large datasets (Klawonn & Höppner,  
287 2003), and the lower limit will be fix in our case to 1. Using the empirical threshold  
288 equation based on the length and dimensions of the dataset proposed by Schwämmle &  
289 Jensen (2010), we found that the superior threshold value of  $m$  for our dataset is around  
290 2.5. By safety, this threshold value is increased by +0.25.

291 As a result, parameter  $m$  will be tested in the interval  $[1; 2.75]$  and  $C$  in the interval  $[2; 8]$ .

292

293

## 294 3. Results and discussion

### 295 3.1 Principal Component Analysis

296 PCA successfully reduced the five original variables (Wind speed toward North and East,  
297 Gust wind speed toward North and East and Rhone discharge) into three components  
298 and gave a summed variance of 96.4% (Fig1 supplementary material). This is not  
299 surprising since the gust wind speed and mean wind speed are correlated due to same  
300 direction (Fig 2 supplementary material. The first axis contains 51% of variability with

301 the information on wind direction. The second axis with 25 % of variability contains the  
302 information on wind speed, and the last one (20% variability) corresponds to the Rhone  
303 discharge. The “elbow criteria”, the “Kaiser rule” and the interpretation of the  
304 components confirm without ambiguity these three components (Fig 1 supplementary  
305 material). The lasting 3.6% carried by the two remaining components concern really  
306 specific and scarce interactions like the anticorrelation between mean wind speed and  
307 gust wind speed.

308 As a result, 80 and 20% of the variability are due to the variations of winds and liquid  
309 discharge respectively.

### 310 3.2 Clustering results and performances

311 Fuzzy-c-mean clustering was performed on the 128262 observations and the three main  
312 dimensions resulting from PCA. A summary on classification performances based on XB  
313 index is shown Fig 2. All configurations performs reasonably well except the one with 3  
314 clusters. An interesting result is that the 2 clusters configuration performed reasonably  
315 well, which confirms that the plume dynamics can be described as a first approach by  
316 considering only the wind direction that is South East against North West winds. This is  
317 in agreement with the 50% of variability held by the wind direction discussed hereunder.  
318 However, the configuration selected is the one giving the better result for XB, with 6  
319 clusters optimized at  $m=2.45$  ( $XB=0.19$ ).

320

### 321 3.3 Characterization of the scenarios

322 A cluster gathers observations having close values for one or more variables. These  
323 properties on variables are specific to each cluster and are then interpreted hereunder as  
324 a scenario.

325 In order to interpret the clustering and to characterize the resulting scenarios we  
326 present the distribution of winds and discharges in Fig 3 and 4, whereas Fig 5 shows the  
327 percentage of occurrence of these scenarios for each month. The discharge distribution in  
328 each cluster was significantly different from the global distribution of Rhone discharge in  
329 Arles based on the Kolmogorov-Smirnov test (see Fig 4).

330 In the description below, a flood event for the Rhone River refers to a discharge above a  
331 threshold set at  $3900\text{m}^3/\text{s}$  in Arles (Boudet et al., 2017). A storm criteria is usually the  
332 significant wave height, but this parameter showed too many breaks in the time series  
333 transmitted in near real time by the buoy over the 2009-2019 period. Also, we defined  
334 sea storm here by using as a threshold the quantile 98 of our offshore gust wind speed  
335 dataset (50.3% of total dataset) which is  $27.8\text{ m/s}$  ( $100\text{ km/h}$ ) (Klawka & Ulbrich, 2003).

336

337 Cluster 1 gathers South-East winds (paragon  $126^\circ$ ) with  $9.2\text{ m/s}$  mean wind-speed and  
338  $16\text{ m/s}$  mean gust. It contains 86% of all observed sea storm events (with the highest  
339 intensity) and 19% of the flood events. The distribution of the hourly water discharge  
340 does not characterize this cluster. Observations belonging to this cluster have less than  
341 6% occurrence in July-September, rising up to 23% in October and November. This  
342 cluster can be interpreted as moderate to high waves scenario resulting from fresh  
343 breeze to violent storm South-East marine winds.

344 Observations in cluster 2 are winds with velocities around  $4.5\text{m/s}$ , and  $9.2\text{ m/s}$  gust fully  
345 coming from the South ( $171^\circ$ ). It contains 12% of all observed sea storm events. It  
346 gathers discharges values under  $2500\text{ m}^3/\text{s}$ , with a median at  $960\text{ m}^3/\text{s}$ . The observations  
347 mainly occur in August-September with 23% occurrence. This cluster can be interpreted  
348 as a Rhone River low flow scenario mainly associated with South-East marine breeze or  
349 sometimes a Sirocco wind coming from the South (Reiter, 1975).

350 Wind observations in cluster 3 show an important variability and are superimposed with  
351 clusters 4 and 5. Most representative winds present a mean speed of 8.5 m/s, and gust  
352 speed of 13.1 m/s. The Rhone discharge distribution for cluster 3 is very different from  
353 the reference distribution (highest Kolmogorov's D statistic). It gathers discharges  
354 higher than 2000 m<sup>3</sup>/s and contains most of the flood events (79% of them). This is also  
355 the cluster showing the highest contrast in seasonality, with an occurrence up to 33%  
356 from November to February, decreasing to 0-2% during the July-October period. Cluster  
357 3 can be interpreted as the "high river flow" scenario with a combination of different  
358 winds coming from the North West.

359

360 In cluster 4, observations are usually winds with 7.2m/s mean wind-speed and 9.1 m/s  
361 mean gust coming from the West (272°). It contains 2% of all observed sea storm events.  
362 Discharges are below 2500 m<sup>3</sup>/s with a median around 1070 m<sup>3</sup>/s. These observations  
363 mainly occur in July-August-September with 33% of occurrence. A specific point is that  
364 their occurrence increases during the afternoon with a peak around 1h AM (Fig 3  
365 supplementary material). Interpretation of this cluster is a Rhone River low flow  
366 scenario gathering moderate sea-breeze coming from the South-West (Cros et al., 2004),  
367 with sometimes a strong onshore gale from West.

368

369 Cluster 5 corresponds to winds with 12.3 m/s average speed and 18.6 m/s gust coming  
370 from a restricted area in the North (325°). The corresponding water discharge  
371 distribution is on the lower part of the global distribution (median of 1140 m<sup>3</sup>/s) and  
372 discharges are always below 3000 m<sup>3</sup>/s. The monthly occurrence is stable (15%) with a  
373 peak in February at 25%. The strong average wind intensities and gust speeds (highest  
374 at 340 °) combined with the restricted wind direction parallel to the Rhone valley stand

375 for the characteristics of the Mistral wind (Reiter, 1975). This last author also found that  
376 the highest peak of occurrence for Mistral is in February. As a result, cluster 5 can be  
377 interpreted as a Mistral wind scenario (dry and strong breeze to strong gale) associated  
378 with low to moderate discharges.

379 Cluster 6\_usually gathers winds with 5.7 m/s average speed, and gusts of 12.5 m/s  
380 coming from the North East (11°). However, winds coming from 340-360° (North/North-  
381 West) are also observed. The related hourly water discharges distribution is in the lower  
382 part of the global one (median of 1230 m<sup>3</sup>/s) and few discharges higher than 3000 m<sup>3</sup>/s  
383 are observed. Occurrence of cluster 6 observations is very stable all along the year,  
384 ranging between 14 and 18 %. This cluster presents the largest gap between the wind  
385 speed average and the gust wind speed, and shows an increasing occurrence in the early  
386 morning. The highest gusts reach 50 m/s and occur episodically in winter with an origin  
387 from 10 to 60°(North-West). These are the strongest gusts observed among all scenarios.  
388 We interpret cluster 6 as a scenario gathering land breeze or valley flow during summer  
389 and winds channeled by Pre Alps mountains (Cros et al., 2004; Duine et al., 2017)which  
390 become stronger in winter (“orsure” according Reiter, 1975)).

391

### 392 3.4 Consequences for surface currents

393

394 Six clear wind/discharge patterns have been identified, but did they correspond or induce  
395 different hydrodynamics responses of the surface currents in the vicinity of the Rhone  
396 River mouth? Consequences for subsurface currents observations issued from the ADCP  
397 on the MesuRho station are investigated through a least squares multiple regression.  
398 Observation membership to clusters  $C_i$  are the explanatory variables and currents in  
399 Eastward and Northward directions are the response variables.

400 Estimators  $X_i$  and  $Y_i$  are then used to calculate current orientation  $\theta$  (rad) and speed  $u$   
401 (m/s) observed on each cluster with equation (1).

402 Confidence intervals are calculated with the robust White standard errors with “lmtest”  
403 package (White, 1980; Hothorn et al., 2019) to avoid heteroscedasticity and  
404 underestimation of confidence intervals. The main current direction for each cluster  
405 obtained by least square regression on memberships is presented on figure 6 (right)  
406 along with the global current rose (left).

407 Currents oriented at  $280^\circ$  correspond to scenario 1 and are in agreement with the more  
408 general modelling and satellite observations during similar south easterlies wind  
409 conditions showing the plume tackled to the Camargue coast (Marsaleix et al., 1998;  
410 Gangloff et al., 2017). Scenario 2 presents small currents not related to the wind  
411 direction. In this case, winds are probably too low and currents are driven by the general  
412 circulation, which has a current speed similar to those of this scenario: 10 cm/s.

413 In scenario 3 the current direction correspond to those at the Rhone River mouth,  
414 meaning that during high water events (discharges superior to  $2500 \text{ m}^3/\text{s}$ ) the river  
415 influence becomes significant.

416 Scenario 4, 5 and 6 seem to follow the surface Ekman transport, with a deflection to the  
417 left relative to the wind direction. Scenario 5 is the one presenting the largest interval of  
418 confidence despite having the straightest wind distribution. A closer look at the data  
419 shows that, in this scenario, the currents deeper than 1.2 m present an important  
420 heterogeneity in their direction. However, for wind average speeds superior to 15 m/s  
421 and gust wind speeds over 25 m/s this heterogeneity does no longer exist and all currents  
422 are oriented in a  $150^\circ$  direction. For comparison, scenario 5 paragon is an average wind  
423 speed of 12.3 m/s and gust wind speed of 18.6 m/s, values which are inferior to the two  
424 thresholds and may explain the currents discrepancies associated with this scenario.

425 To conclude, each scenario has its own current direction and intensity, statistically  
426 different and significant.

427

### 428 3.5 Application

429

430 The main objective of this work is to define the general trends of dispersal in the GoL  
431 that can be expected in the case of artificial radionuclides release within the river. Since  
432 releases may occur at any time in a year, we modeled the dispersion of a radioactive  
433 plume in the GoL for each of the previous hydrodynamic scenario, in order to get an  
434 overview of the potential impacts, whatever the hydrodynamic and climatological  
435 conditions.

436 The simulation code used at IRSN for the marine area is STERNE (“Simulation du  
437 Transport et du transfert d'Eléments Radioactifs dans l'environnement marin”, or  
438 “Simulation of radionuclide transport and transfer in marine environments”). It was  
439 designed to assess the radiological impact of accidental releases affecting the marine  
440 environment. Eulerian radionuclide dispersion is calculated using a tracer advection  
441 diffusion equation. More details on the code can be found in Duffa et al. (2016).

442 We use the 2010 hydrodynamic outputs provided by IFREMER with its MARS3D model  
443 implemented on the North-western Mediterranean Sea (Nicolle et al., 2009). The  
444 simulations assumed a release of 1 TBq of  $^{137}\text{Cs}$  dissolved activity in the river, over a  
445 temporal window of 48 h.  $^{137}\text{Cs}$  was chosen because this radionuclide is released at each  
446 nuclear accident and is also found in authorized releases from nuclear powerplants. This  
447 radionuclide presents a high radiotoxicity (Garnier-Laplace et al., 2011) and is relatively  
448 soluble in seawater with a  $K_d$  ranging from 450 to 2000 L/kg (Delaval et al., 2020). For  
449 comparison, the estimated average direct discharge of  $^{137}\text{Cs}$  to the ocean during the  
450 Fukushima Daiichi nuclear power plants was around 5000 TBq (Buesseler et al., 2017).

451 The simulations were done for each hydro-meteorological scenario defined on the basis of  
452 the 2009-2019 dataset and the plume extension in the GoL was modelled for each  
453 scenario. Since the hydrodynamic inputs are only available for the year 2010, we selected  
454 in this input the most representative temporal window for each scenario simulation by  
455 integrating observations memberships over a sliding window of 48h. The temporal  
456 window presenting the highest summed membership values were selected for each  
457 cluster.

458 The results of the 6 simulations are very different in terms of plume shape and thus  
459 affected areas (Fig 7). Mean winds and discharges conditions over 48 h hours are  
460 indicated in the figure. It must be noted that these values are specific to the chosen  
461 temporal windows, and thus can be different from the parangons presented in the  
462 previous chapter.

463 In scenario 1 (strong marine wind with moderate discharge conditions), the plume is  
464 constrained to the coast and extends west in agreement with the currents at the buoy.  
465 This scenario has already been highlighted by Demarcq & Wald, (1984) and Many et al.,  
466 (2018) or modelled by Estournel et al., (1997). A part of the activity remains blocked in  
467 the estuary due to winds in opposition with its flowing path and an increase in sea level  
468 at the mouth limiting the power of the jet.

469 The lowest expansion of the plume is observed with scenario 2 (weak wind with  
470 discharge slightly under the annual mean). The plume has the lowest surface spatial  
471 expansion among the 6 plumes and is nearly stagnant and remains with a high activity.  
472 This is in agreement with the currents observed at the buoy showing really low speeds.  
473 This scenario appears mostly during summer (Fig 4), and satellite images confirmed that  
474 the turbid plume present effectively its smallest area at this period (Gangloff et al.  
475 (2017).

476 Scenario 3 corresponds to a high Rhone River discharge and northwest winds conditions.  
477 The plume presents a large area but the northwesterly wind is powerful enough to carry  
478 the plume offshore. For different wind stress simulations, Marsaleix et al., (1998)  
479 showed that winds around 30 km/h were sufficient to detach the plume from the coast.  
480 According to this author this threshold is independent of Rhone River discharge.

481 In scenario 4 (strong westerly wind and low discharge conditions), the plume extends  
482 over a large area favored by the presence of a summer stratification at low discharge. A  
483 part of the plume at the latitude of the buoy can be deflected eastwards in the Gulf of  
484 Fos, in agreement with current data at the buoy. According to Fraysse et al., (2014) this  
485 plume shape is the first step toward an intrusion in the Bay of Marseille if this scenario  
486 is followed by south east winds conditions. To note, such intrusions occurred in summer  
487 (Fraysse et al, 2014) when the probability of occurrence of this scenario are the highest.

488 In scenario 5, with a strong northwest wind (Mistral) and low discharge conditions the  
489 plume stands out from the coast as shown by Demarcq & Wald, (1984) and Gangloff et  
490 al., (2017) and modelled by Estournel et al., (1997). This case is favorable to an export of  
491 the plume far away from the coast, even at low discharge conditions and moderate  
492 Mistral (but the wind speed are however above the 30 km/h threshold proposed by  
493 Marsaleix et al., (1998)).

494 Finally, the northeast wind and moderate discharge conditions of scenario 6 maintain  
495 the plume towards the coast, similarly to scenario 1. It is here again in agreement with  
496 the currents measured at the buoy. This is confirmed by Gangloff et al., (2017) who  
497 showed that for the most northern winds (higher than 340 °) the plume tends to be  
498 tacked to the coast .The part of the plume going East towards the gulf of Fos is quite  
499 unexpected. A closer look at the dataset shows that this temporal window of 48 h,  
500 despite being classified as scenario 6, presented 16 consecutives observations (8 hours

501 period)corresponding to scenario 2. This explains why the plume extends toward the gulf  
502 of Fos in a similar fashion as in scenario 2.

503

504 All these simulations shown that the activity plume may be maintained along the  
505 western coast of the Rhone river outlet (Scenarios 1 and 6), its eastern side (Scenario 4)  
506 or can extend far away from the coast (Scenario 5). Plume of different extents can also  
507 remain nearly stable (Scenarios 2 and 3) until a change of hydrodynamic, conditions and  
508 thus scenario (most likely shifts from 2 to 4, 5, 6 and from 3 to 5, 6, 1).

509

510

511 Each cluster of hydrodynamic forcings has thus its own patterns for Rhone River plume  
512 spreading in the GoL. Their hydrodynamic variables and resulting trends were  
513 presented in the previous chapters, and these results now allow to better evaluate the  
514 risk of propagation of  $^{137}\text{Cs}$  activity. However, it is also interesting to define thresholds  
515 values for these variables, in order to be able to select the most appropriate scenario to  
516 apply in case of alert on accidental release of radionuclides (or any kind of chemical  
517 contaminants). To summarize the differences obtained between the scenarios, a  
518 simplified decision tree has been constructed (Fig 8). From top to bottom it allows to  
519 outline practical separation criteria (Fig 8).

520 The classification of these 6 scenarios is based on the wind (and gust) direction, wind  
521 speed and water discharge. These *in situ* conditions can thus be associated with a  
522 scenario in near real-time, as they are available at this time scale from the websites of  
523 Coriolis Cotier (wind) and Vigicrues (river flow). The tree reproduces the classification  
524 using 80% of the hydrodynamic raw data (without PCA treatment) as training, and 20%  
525 as a validation set. It allows a fast crisp classification into one of the 6 established  
526 scenario with 83% of accuracy on both trained and tested data. As an example, in case of

527 wind direction of 270° and a river discharge of 2500 m<sup>3</sup>/s, the shape of the plume will  
528 correspond to scenario 3. Currents directions at the buoy (Coriolis Cotier) can also be  
529 used as an additional verification.

## 530 Conclusion

531

532 In this paper, a 10-year period was considered in order to identify the main combinations  
533 of hydrodynamic forcings (wind and Rhone River discharge) using a fuzzy c-mean  
534 clustering. These combinations, called scenario summarized mean shelf behavior  
535 providing a very important information to estimate and understand the Rhone plume  
536 patterns in case of accidental release. In addition, existence of observations memberships  
537 allowed to spot the best temporal windows to run simulations covering all possible  
538 patterns.

539 6 scenarios have been identified and simulations showed that the plume behavior was  
540 different for each of them. These plume patterns are more or less critical in terms of  
541 radiologic risks regarding the areas affected and the dilution of the activity. If  
542 necessary, wind speed measured on one point are sufficient to extrapolate plume shape  
543 for 48 hours on this zone, and the surface currents measured at the Roustan buoy will  
544 give a first idea of plume orientation. This study provided a first global picture of main  
545 Rhone River plume patterns and consequences for radionuclides accidental releases, but  
546 the methodology may be applied to other estuaries.

547

## 548 Acknowledgements

549 The authors are indebted to the Institute for Radiological Protection and Nuclear Safety  
550 (IRSN) and to Region Sud (Provence-Alpes-Côte d'Azur) authorities for the PhD funding.  
551 This study was conducted within the Rhône Sediment Observatory (OSR) program, a  
552 multi-partner research program funded through Plan Rhône of the European Regional

553 Development Fund (ERDF), Agence de l'Eau Rhône Méditerranée Corse, CNR, EDF and  
554 three regional councils (Région Auvergne-Rhône-Alpes, PACA and Occitanie). The  
555 Mesurho station is part of the COAST-HF network and associates IFREMER, IRSN,  
556 CNRS, CETMEF, and CEREMA..

557

558

## 559 References

560 Bárcena, J. F., Camus, P., García, A., & Álvarez, C., 2015. Selecting model scenarios of  
561 real hydrodynamic forcings on mesotidal and macrotidal estuaries influenced by  
562 river discharges using K-means clustering. *Environmental Modelling and Software*,  
563 68, 70–82. <https://doi.org/10.1016/j.envsoft.2015.02.007>

564 Ben-Dor, A., Shamir, R., & Yakhini, Z., 2004. Clustering Gene Expression Patterns.  
565 *Journal of Computational Biology*, 6 (3–4).  
566 [https://doi.org/https://doi.org/10.1089/106652799318274](https://doi.org/10.1089/106652799318274)

567 Bezdek, J. C. 1981. *Pattern recognition with Fuzzy Objective Function Algorithms*  
568 (Springer (ed.); Plenum Pre). <https://doi.org/10.1007/978-1-4757-0450-1>

569 Boudet, L., Sabatier, F., & Radakovitch, O. 2017., Modelling of sediment transport  
570 pattern in the mouth of the Rhone delta: Role of storm and flood events. *Estuarine,*  
571 *Coastal and Shelf Science*, 198, 568–582. <https://doi.org/10.1016/j.ecss.2016.10.004>

572 Buesseler, K., Dai, M., Aoyama, M., Benitez-Nelson, C., Charmasson, S., Higley, K.,  
573 Maderich, V., Masqué, P., Morris, P. J., Oughton, D., & Smith, J. N., 2017.  
574 Fukushima Daiichi–Derived Radionuclides in the Ocean: Transport, Fate, and  
575 Impacts. *Annual Review of Marine Science*, 9 (1), 173–203.  
576 <https://doi.org/10.1146/annurev-marine-010816-060733>

577 Campello, R. J. G. B., & Hruschka, E. R., 2006. A fuzzy extension of the silhouette width  
578 criterion for cluster analysis. *Fuzzy Sets and Systems*, 157 (21), 2858–2875.  
579 <https://doi.org/10.1016/j.fss.2006.07.006>

580 Chaimontree, S., Atkinson, K., & Coenen, F., 2010. Advanced Data Mining and  
581 Applications Part 1. In Springer (Ed.), *Advanced Data Mining and Applications Part*  
582 *1* (p. 625).

583 Charmasson, S., Barker, E., Calmet, D., Pruchon, A. S., & Thébault, H., 1999. Long-term  
584 variations of man-made radionuclide concentrations in a bio- indicator *Mytilus*  
585 *gallopro incialis* from the French Mediterranean coast. *Science of the Total*  
586 *Environment*, 237–238, 93–103. [https://doi.org/10.1016/S0048-9697\(99\)00127-8](https://doi.org/10.1016/S0048-9697(99)00127-8)

587 Cros, B., Durand, P., Cachier, H., Drobinski, P., Fréjafon, E., Kottmeier, C., Perros, P. E.,  
588 Peuch, V. H., Ponche, J. L., Robin, D., Saïd, F., Toupance, G., & Wortham, H., 2004.  
589 The ESCOMPTE program: An overview. *Atmospheric Research*, 69(3–4), 241–279.  
590 <https://doi.org/10.1016/j.atmosres.2003.05.001>

591 Delaval, A., Duffa, C., & Radakovitch, O., 2020. A review on cesium desorption at the  
592 freshwater-seawater interface. *Journal of Environmental Radioactivity*, 218,  
593 106255. <https://doi.org/10.1016/j.jenvrad.2020.106255>

594 Demarcq, H., & Wald, L., 1984. La dynamique superficielle du panache du Rhône d '   
595 après l ' imagerie infrarouge satellitaire. *Oceanologica Acta*, 7(2), 159–162.  
596 <http://hal.archives-ouvertes.fr/hal-00464192/>

597 Diaz, F., Bănaru, D., Verley, P., & Shin, Y. J., 2019. Implementation of an end-to-end  
598 model of the Gulf of Lions ecosystem (NW Mediterranean Sea). II. Investigating the  
599 effects of high trophic levels on nutrients and plankton dynamics and associated  
600 feedbacks. *Ecological Modelling*, 405, 51–68.  
601 <https://doi.org/10.1016/j.ecolmodel.2019.05.004>

602 Duffa, C., Bailly, P., Caillaud, M., Charmasson, S., & Renaud, P., 2016. Development of  
603 emergency response tools for accidental radiological contamination of French  
604 coastal areas. *Journal of Environmental Radioactivity* 151, 487–494.  
605 <https://doi.org/10.1016/j.jenvrad.2015.04.019>

606 Duine, G. J., Hedde, T., Roubin, P., Durand, P., Lothon, M., Lohou, F., Augustin, P., &  
607 Fourmentin, M., 2017. Characterization of valley flows within two confluent valleys  
608 under stable conditions: observations from the KASCADE field experiment.  
609 *Quarterly Journal of the Royal Meteorological Society*, 143 (705), 1886–1902.  
610 <https://doi.org/10.1002/qj.3049>

611 Dunn, J. C., 1974. Well-Separated Clusters and Optimal Fuzzy Partitions. *Journal of*  
612 *Cybernetics*, 4 (1), 95–104. <https://doi.org/10.1080/01969727408546059>

613 Durrieu De Madron, X., Abassi, A., Heussner, S., Monaco, A., Aloisi, J. C., Radakovitch,  
614 O., Giresse, P., Buscail, R., & Kerherve, P., 2000. Particulate matter and organic  
615 carbon budgets for the Gulf of Lions (NW Mediterranean). *Oceanologica Acta*, 23(6),  
616 717–730. [https://doi.org/10.1016/S0399-1784\(00\)00119-5](https://doi.org/10.1016/S0399-1784(00)00119-5)

617 Estournel, C., Kondrachoff, V., Marsaleix, P., & Vehil, R., 1997. The plume of the Rhone:  
618 Numerical simulation and remote sensing. *Continental Shelf Research*, 17(8), 899–  
619 924. [https://doi.org/10.1016/S0278-4343\(96\)00064-7](https://doi.org/10.1016/S0278-4343(96)00064-7)

620 Eyrolle, F., Lepage, H., Antonelli, C., Morereau, A., Cossonnet, C., Boyer, P., &  
621 Gurriaran, R., 2020. Radionuclides in waters and suspended sediments in the  
622 Rhone River (France) - Current contents, anthropic pressures and trajectories.  
623 *Science of The Total Environment*, 137873.  
624 <https://doi.org/10.1016/j.scitotenv.2020.137873>

625 Falcieri, F. M., Benetazzo, A., Sclavo, M., Russo, A., & Carniel, S., 2014. Po River plume  
626 pattern variability investigated from model data. *Continental Shelf Research*, 87,

627 84–95. <https://doi.org/10.1016/j.csr.2013.11.001>

628 Ferraro, M. B., & Giordani, P., 2015. A toolbox for fuzzy clustering using the R  
629 programming language. *Fuzzy Sets and Systems*, 279, 1–16.  
630 <https://doi.org/10.1016/j.fss.2015.05.001>

631 Fraysse, M., Pairaud, I., Ross, O. N., Faure, V. M., & Pinazo, C., 2014. Journal of  
632 Geophysical Research: Oceans Generation processes and impacts on ecosystem  
633 functioning. *Journal of Geophysical Research: Oceans*, 6535–6556.  
634 <https://doi.org/10.1002/2014JC010022>.Received

635 Fu Lai, C., & Tong, L., 1994. Fuzzy Competitive Learning. *Neural Networks* . 7 (3), 539–  
636 551.

637 Gangloff, A., Verney, R., Doxaran, D., Ody, A., & Estournel, C., 2017. Investigating  
638 Rhône River plume (Gulf of Lions, France) dynamics using metrics analysis from  
639 the MERIS 300m Ocean Color archive (2002–2012). *Continental Shelf Research*,  
640 144, 98–111. <https://doi.org/10.1016/j.csr.2017.06.024>

641 Garnier-Laplace, J., Beaugelin-Seiller, K., & Hinton, T. G., 2011. Fukushima wildlife  
642 dose reconstruction signals ecological consequences. *Environmental Science and  
643 Technology*, 45 (12), 5077–5078. <https://doi.org/10.1021/es201637c>

644 Gontier, G., Grenz, C., Calmet, D., & Sacher, M. (1992). The contribution of *Mytilus* sp.  
645 in radionuclide transfer between water column and sediments in the estuarine and  
646 delta systems of the Rhône river. *Estuarine, Coastal and Shelf Science*, 34 (6), 593–  
647 601. [https://doi.org/10.1016/S0272-7714\(05\)80064-2](https://doi.org/10.1016/S0272-7714(05)80064-2)

648 Hornik, K., Weingessel, A., Leisch, F., 2019. *Package ‘e1071.’*

649 Hothorn, T., Zeileis, A., Farebrother, R. W., Cummins, C., Millo, G., & Mitchell, D., 2019.  
650 *Testing Linear Regression Models (Package ‘lmtest’)*.

651 Husson, F., Josse, J., & Pagès, J., 2010. *Technical Report – Agrocampus. September.*

652 Jain, A. K., Murty, M. N., & Flynn, P. J., 1999. Data clustering: A review. *ACM*  
653 *Computing Surveys*, 31 (3), 264–323. <https://doi.org/10.1145/331499.331504>

654 Kaufmann, P., & Whiteman, C. D., 1999. Cluster-analysis classification of wintertime  
655 wind patterns in the Grand Canyon region. *Journal of Applied Meteorology*, 38 (8),  
656 1131–1144. [https://doi.org/10.1175/1520-0450\(1999\)038<1131:cacoww>2.0.co;2](https://doi.org/10.1175/1520-0450(1999)038<1131:cacoww>2.0.co;2)

657 Kim, H. S., Kim, J. H., Ho, C. H., & Chu, P. S., 2011. Pattern classification of typhoon  
658 tracks using the fuzzy c-means clustering method. *Journal of Climate*, 24(2), 488–  
659 508. <https://doi.org/10.1175/2010JCLI3751.1>

660 Klawa, M., & Ulbrich, U., 2003. A model for the estimation of storm losses and the  
661 identification of severe winter storms in Germany. *Natural Hazards and Earth*  
662 *System Science*, 3 (6), 725–732. <https://doi.org/10.5194/nhess-3-725-2003>

663 Klawonn, F., & Höppner, F., 2003. What is fuzzy about fuzzy clustering? Understanding  
664 and improving the concept of the fuzzifier. In Springer (Ed.), *Advances in Intelligent*  
665 *Data Analysis* (Vol. 1716, pp. 254–263). <https://doi.org/10.1108/ir.1999.04926fae.001>

666 Kovács, J., Bodnár, N., & Török, Á., 2016. The application of multivariate data analysis  
667 in the interpretation of engineering geological parameters. *Open Geosciences*, 8 (5),  
668 52–61. <https://doi.org/10.1515/geo-2016-0005>

669 Launay, M., Dugué, V., Faure, J. B., Coquery, M., Camenen, B., & Le Coz, J., 2019.  
670 Numerical modelling of the suspended particulate matter dynamics in a regulated  
671 river network. *Science of the Total Environment*, 665, 591–605.  
672 <https://doi.org/10.1016/j.scitotenv.2019.02.015>

673 Lê, S., Josse, J., & Husson, F., 2008. FactoMineR: An R package for multivariate  
674 analysis. *Journal of Statistical Software*, 25(1), 1–18.

675 <https://doi.org/10.18637/jss.v025.i01>

676 Liu, Y., Li, Z., Xiong, H., Gao, X., & Wu, J., 2010. Understanding of internal clustering  
677 validation measures. *Proceedings - IEEE International Conference on Data Mining,*  
678 *ICDM*, 911–916. <https://doi.org/10.1109/ICDM.2010.35>

679 Ludwig, W., Dumont, E., Meybeck, M., & Heussner, S., 2009. River discharges of water  
680 and nutrients to the Mediterranean and Black Sea: Major drivers for ecosystem  
681 changes during past and future decades? *Progress in Oceanography*, 80 (3–4), 199–  
682 217. <https://doi.org/10.1016/j.pocean.2009.02.001>

683 MacQueen, J., 1965. Some methods for classification and analysis of multivariate  
684 observations. *Proceedings of the Fifth Berkeley Symposium on Mathematical*  
685 *Statistics and Probability*, 281–297.

686 Many, G., Bourrin, F., Durrieu de Madron, X., Ody, A., Doxaran, D., & Cauchy, P., 2018.  
687 Glider and satellite monitoring of the variability of the suspended particle  
688 distribution and size in the Rhône ROFI. *Progress in Oceanography*, 163, 123–135.  
689 <https://doi.org/https://doi.org/10.1016/j.pocean.2017.05.006>

690 Marsaleix, P., Estournel, C., Kondrachoff, V., & Vehil, R., 1998. A numerical study of the  
691 formation of the Rhone River plume. *Journal of Marine Systems*, 14 (1–2), 99–115.  
692 [https://doi.org/10.1016/S0924-7963\(97\)00011-0](https://doi.org/10.1016/S0924-7963(97)00011-0)

693 Martin, D., Pititto, F., Gil, J., Mura, M. P., Bahamon, N., Romano, C., Thorin, S.,  
694 Schvartz, T., Dutrieux, É., & Bocquet, Y., 2019. Long-distance influence of the  
695 Rhône River plume on the marine benthic ecosystem: Integrating descriptive  
696 ecology and predictive modelling. *Science of the Total Environment*, 673, 790–809.  
697 <https://doi.org/10.1016/j.scitotenv.2019.04.010>

698 Millot, C., 1990. The Gulf of Lions' hydrodynamics. *Continental Shelf Research*, 10(9–

699 11), 885–894. [https://doi.org/10.1016/0278-4343\(90\)90065-T](https://doi.org/10.1016/0278-4343(90)90065-T)

700 Millot, C., 1999. Circulation in the Western Mediterranean Sea. *Journal of Marine*  
701 *Systems*, 20 (1–4), 423–442. [https://doi.org/10.1016/S0924-7963\(98\)00078-5](https://doi.org/10.1016/S0924-7963(98)00078-5)

702 Napoleon, D., & Pavalakodi, S., 2011. A New Method for Dimensionality Reduction  
703 Using KMeans Clustering Algorithm for High Dimensional Data Set. *International*  
704 *Journal of Computer Applications*, 13(7), 41–46. <https://doi.org/10.5120/1789-2471>

705 Nicolle, A., Garreau, P., & Liorzou, B., 2009. Modelling for anchovy recruitment studies  
706 in the Gulf of Lions (Western Mediterranean Sea). *Ocean Dynamics*, 59 (6), 953–  
707 968. <https://doi.org/10.1007/s10236-009-0221-6>

708 Pairaud, I. L., Gatti, J., Bensoussan, N., Verney, R., & Garreau, P., 2011. Hydrology and  
709 circulation in a coastal area off Marseille: Validation of a nested 3D model with  
710 observations. *Journal of Marine Systems*, 88(1), 20–33.  
711 <https://doi.org/10.1016/j.jmarsys.2011.02.010>

712 Pairaud, I. L., Lyard, F., Auclair, F., Letellier, T., & Marsaleix, P., 2008. Dynamics of the  
713 semi-diurnal and quarter-diurnal internal tides in the Bay of Biscay. Part 1:  
714 Barotropic tides. *Continental Shelf Research*, 28 (10–11), 1294–1315.  
715 <https://doi.org/10.1016/j.csr.2008.03.004>

716 Pairaud, I., Repecaud, M., Ravel, M., Fuchs, R., Arnaud, M., Champelovier, A.,  
717 Rabouille, C., Bomble, B., Toussaint, F., Garcia, F., Raimbault, P., Verney, R.,  
718 Meule, S., Gaufres, P., Bonnat, A., & Cadiou, J., 2016. Plateforme instrumentée de  
719 suivi des paramètres environnementaux à l’embouchure du Rhône. *Mesures à haute*  
720 *résolution dans l’environnement marin côtier (CNRS Alpha)*, pp. 73–87.

721 Ramze Rezaee, M., Lelieveldt, B. P. F., & Reiber, J. H. C., 1998. A new cluster validity  
722 index for the fuzzy c-mean. *Pattern Recognition Letters*, 19 (3–4), 237–246.

723 [https://doi.org/10.1016/S0167-8655\(97\)00168-2](https://doi.org/10.1016/S0167-8655(97)00168-2)

724 Reffray, G., Fraunié, P., & Marsaleix, P., 2004. Secondary flows induced by wind forcing  
725 in the Rhône region of freshwater influence. *Ocean Dynamics*, *54*(2), 179–196.  
726 <https://doi.org/10.1007/s10236-003-0079-y>

727 Reiter, E. R., 1975. Technical report .Weather phenomena of the mediterranean basin  
728 Part I: General description of the meteorological processes. U.S. department of  
729 Commerce. Springfield

730 Renner, R. M., 1993. The Resolution of a Compositional Data Set into Mixtures of a  
731 Fixed Source Compositions. *Applied Statistics*, *42* (4), 615–631.  
732 <https://doi.org/https://doi.org/10.2307/2986179>

733 Sanchez-Cabeza, J.-A., Molero, J., Merino, J., Pujol, L., & Mitchell, P. I., 1992. 137 Cs as  
734 a tracer of the Catalan current. *Oceanologica Acta*, *18*(2), 221–226.

735 Schwämmle, V., & Jensen, O. N., 2010. A simple and fast method to determine the  
736 parameters for fuzzy c-means cluster analysis. *Bioinformatics*, *26* (22), 2841–2848.  
737 <https://doi.org/10.1093/bioinformatics/btq534>

738 Selim, S. Z., & Kamel, M., 1992. On the mathematical and numerical properties of the  
739 fuzzy c-means algorithm. *49*, 181–191.

740 Setnes, M., & Babuška, R., 1999. Fuzzy relational classifier trained by fuzzy clustering.  
741 *IEEE Transactions on Systems, Man, and Cybernetics, Part B: Cybernetics*, *29* (5),  
742 619–625. <https://doi.org/10.1109/3477.790444>

743 Tomczak, W., Boyer, P., Krimissa, M., & Radakovitch, O., 2019. Applied Geochemistry .K  
744 d distributions in freshwater systems as a function of material type , mass- volume  
745 ratio , dissolved organic carbon and pH. *105* (April), 68–77.

746 Ulses, C., Estournel, C., Puig, P., Durrieu de Madron, X., & Marsaleix, P., 2008. Dense

747 shelf water cascading in the northwestern Mediterranean during the cold winter  
748 2005: Quantification of the export through the Gulf of Lion and the Catalan margin.  
749 Geophysical Research Letters, 35 (7), 2–7. <https://doi.org/10.1029/2008GL033257>

750 Wang, W., & Zhang, Y., 2007. On fuzzy cluster validity indices. *Fuzzy Sets and Systems*,  
751 158(19), 2095–2117. <https://doi.org/10.1016/j.fss.2007.03.004>

752 White, H., 1980. A Heteroskedasticity-Consistent Covariance Matrix Estimator and a  
753 Direct Test for Heteroskedasticity. *Econometrica*, 48(4), 817.  
754 <https://doi.org/10.2307/1912934>

755 Xie, X. L., & Beni, G., 1991. A validity measure for fuzzy Clustering. *IEEE Transactions*  
756 *on Pattern Analysis and Machine Intelligence*, 13 (8), 841–847.

757 Xu, C., Xu, Y., Hu, J., Li, S., & Wang, B., 2019. A numerical analysis of the summertime  
758 Pearl River plume from 1999 to 2010: Dispersal patterns and intraseasonal  
759 variability. *Journal of Marine Systems*, 192 (November 2018), 15–27.  
760 <https://doi.org/10.1016/j.jmarsys.2018.12.010>

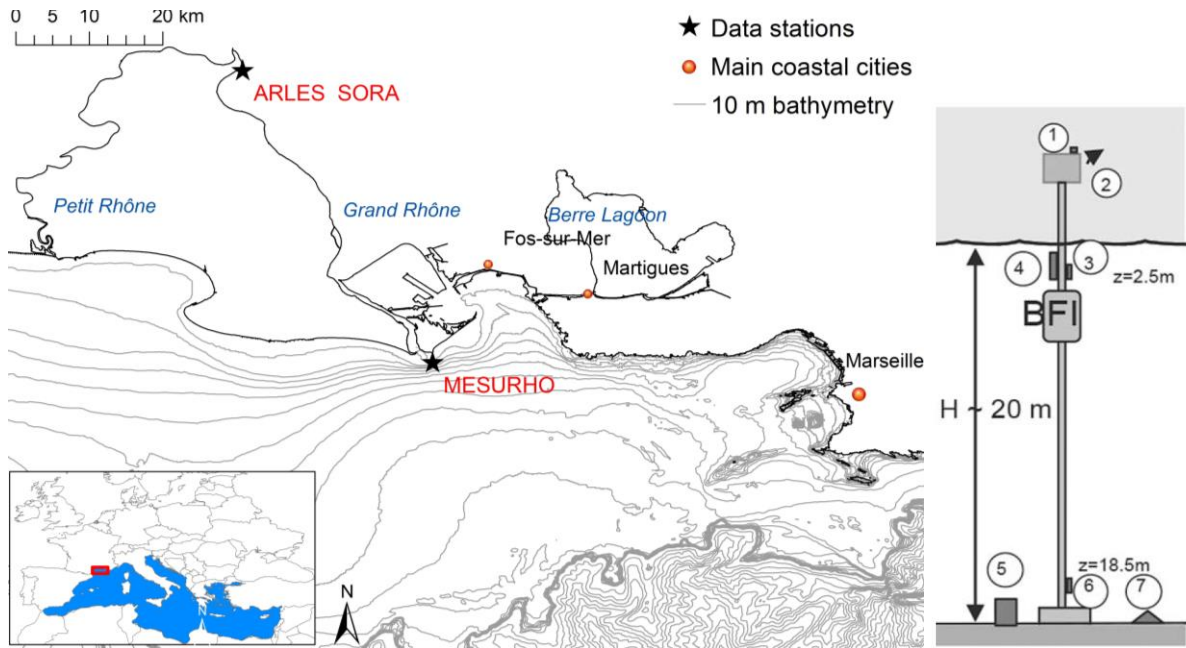
761 Yadav, J., & Sharma, M., 2013. A Review of K-mean Algorithm. *International Journal of*  
762 *Engineering Trends and Technology*, 4 (7), 2972–2976.

763 Zadeh, L. A., 1965. Fuzzy Sets \*. *Information and control* (8), 338–353.

764 Zhang, G., Wang, Y., Zhang, J., & Niu, Y., 2011. Study on flood clustering and  
765 recognition methods based on fuzzy set theory. 2011 Eighth International  
766 Conference on Fuzzy Systems and Knowledge Discovery (FSKD), 887–891.  
767 <https://doi.org/10.1109/FSKD.2011.6019681>

768

769

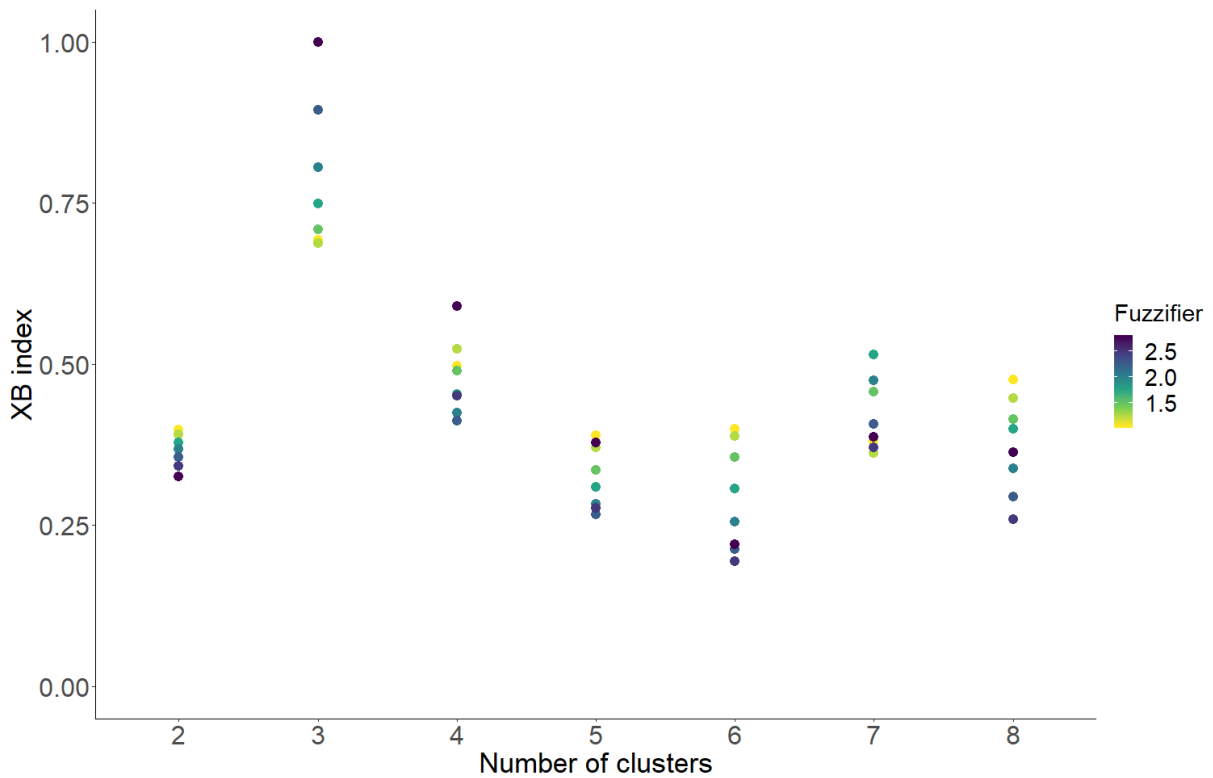


770

771 *Fig 1 : Map of the GoL (Mediterranean sea) and Rhone River estuary indicating the*  
 772 *locations of discharge and weather stations used in the fuzzy-clustering algorithm.*

773 *Scheme of MesuRhO buoy devices Weather station + PAR (1), solar panels and*  
 774 *control and transmission automat ABIN (2), Multiparameters sonds (3 and 6)*  
 775 *nitrates captor ISUS (4), benthic station (5), ADCP (7).*

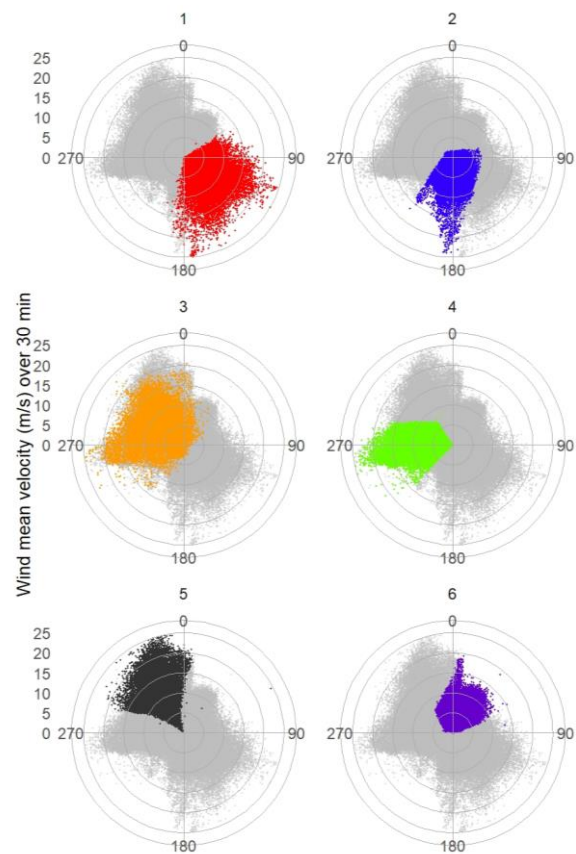
776



777

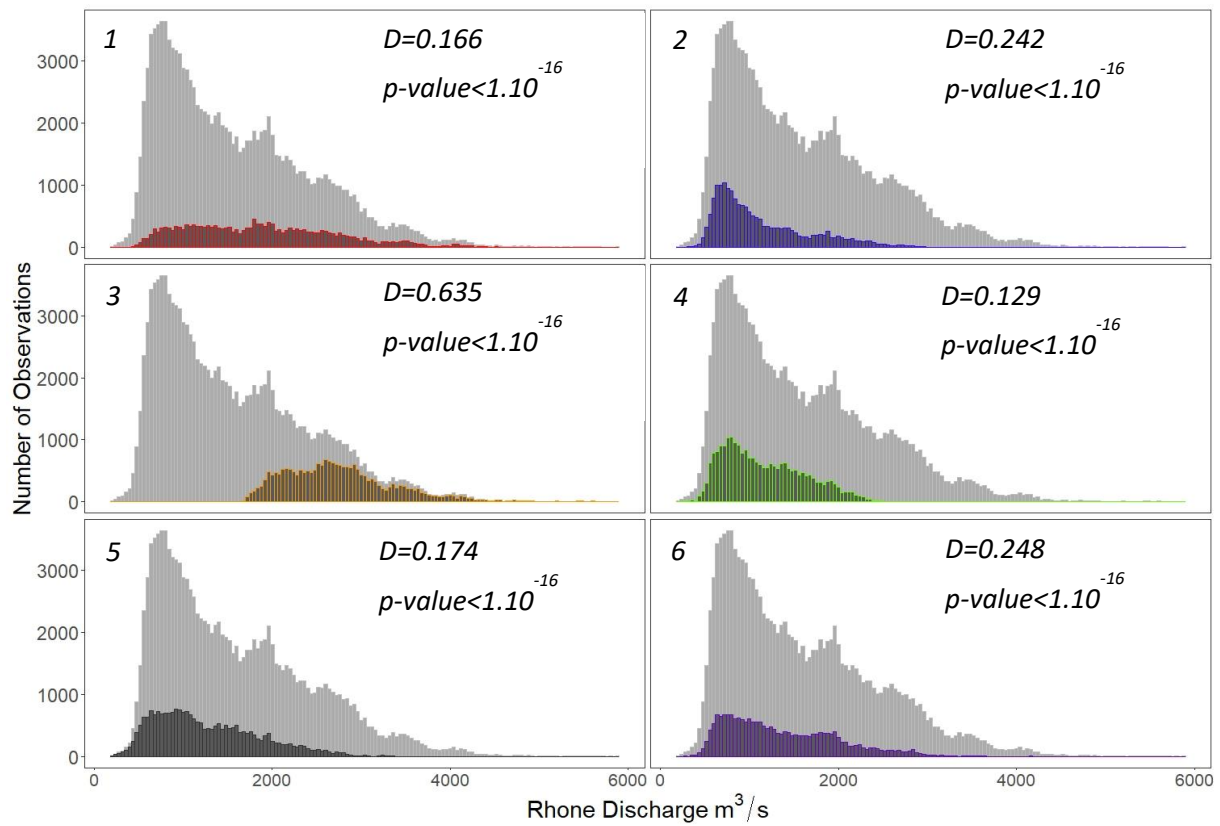
778 *FIG 2 : XIE AND BENI INDEX VALUES FOR DIFFERENT {C,M} SIMULATIONS WITH FUZZY C-*  
 779 *MEAN ALGORITHM. A LOWER INDEX INDICATES A BETTER CLASSIFICATION.*

780  
781  
782  
783  
784  
785  
786



787  
788  
789  
790  
791  
792  
793  
794  
795

*Fig 3: Grey dots: mean wind origin and speed (m/s) over 30 min from 2009 to 2019 measured at the Mesurho buoy, in front of the Rhone river. Color dots: cluster mean wind and speed sub-distributions.*



796

797

798

799

800

801

802

803

804

805

806

807

808

809

810

*Fig 4 : Rhône river hourly discharge (SORA, Arles) from 2009 to 2019 distribution (grey) and cluster Rhône discharge sub-distributions. Results from two-sample Kolmogorov-Smirnov test are shown. D statistic indicates how the distribution in each cluster is different from the reference distribution (all Rhône discharge values) Higher values of D indicates larger differences.*

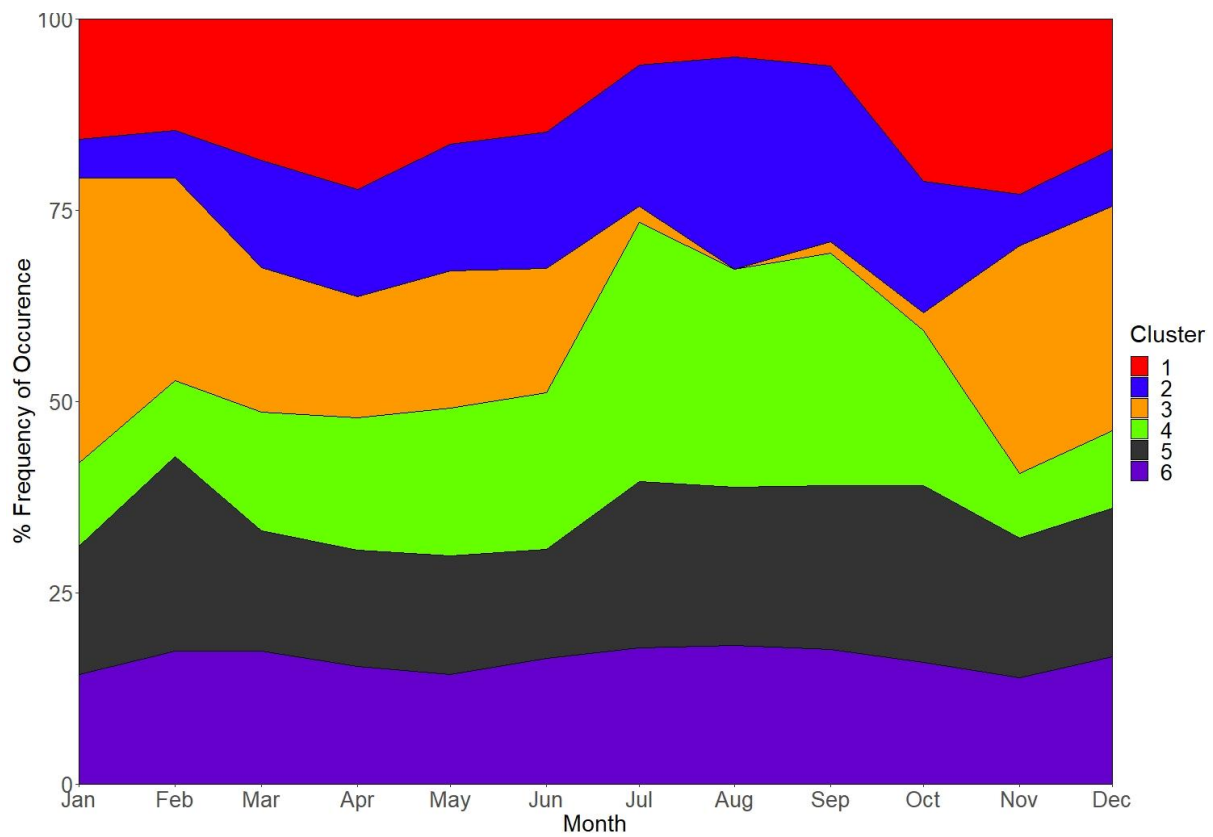
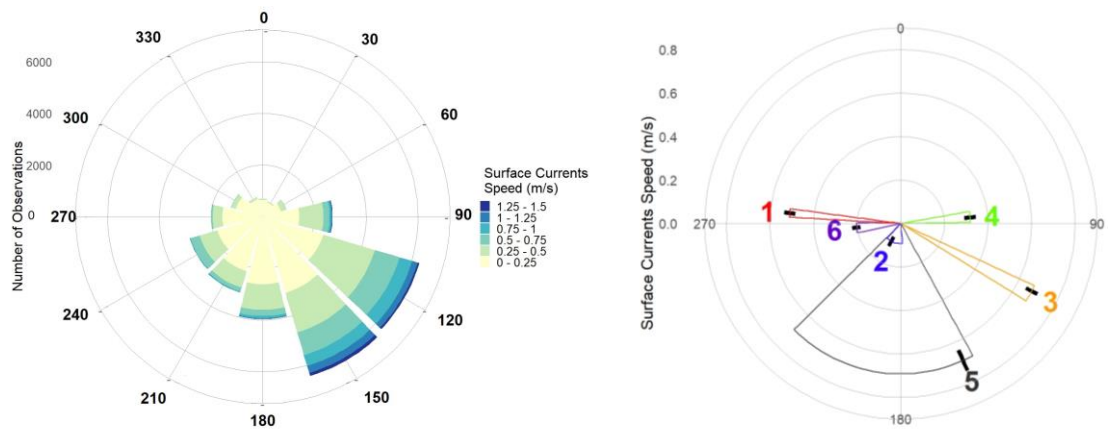


Fig 5: Monthly occurrence of the 6 different scenarios over the 2009-2019 period.

811  
 812  
 813  
 814  
 815  
 816  
 817  
 818  
 819  
 820  
 821  
 822  
 823  
 824  
 825  
 826  
 827



828

829

830

831

832

833

834

835

836

837

838

839

840

841

842

843

844

845

846

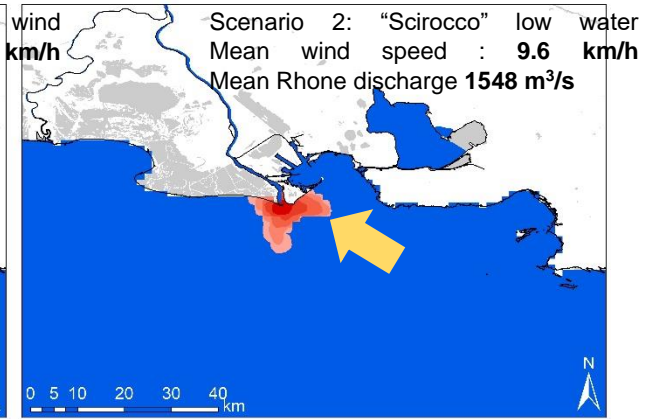
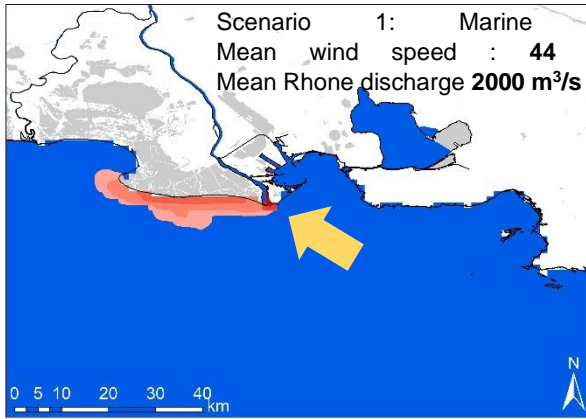
847

848

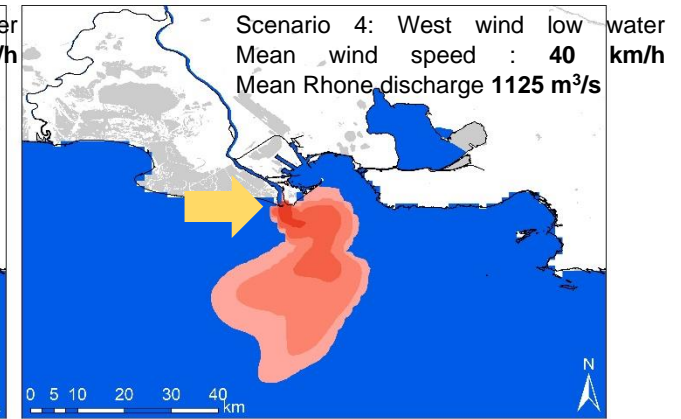
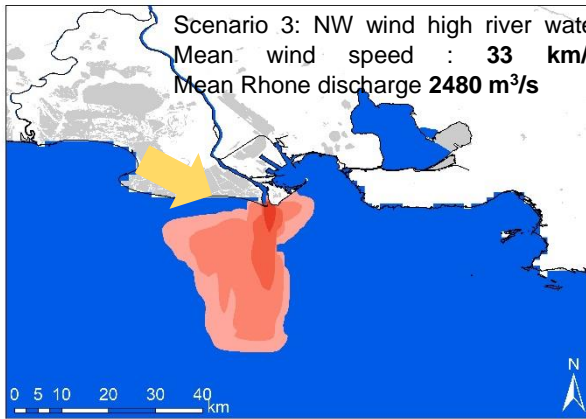
849

*Fig 6: Surface currents (depth<1.5m) direction and module measured at the Mesurho (a) buoy and main direction (thick black dashes) and current speed for each scenario (b) obtained by least square regression. Confidence intervals are for  $\alpha=0.05$*

850

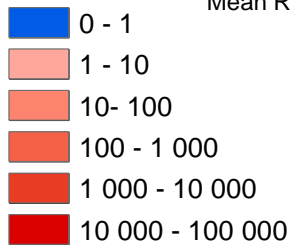


851

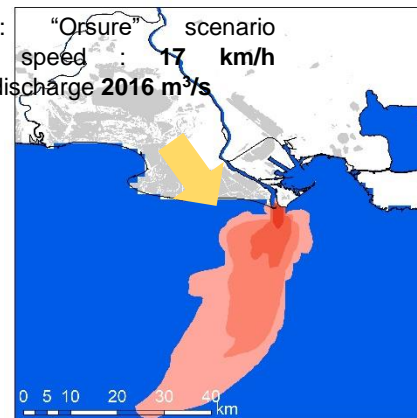


Activity in seawater (Bq/m<sup>3</sup>)

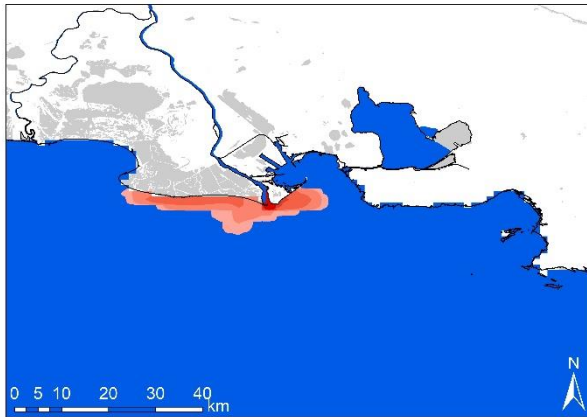
Scenario 5: "Mistral" scenario  
Mean wind speed : 46 km/h  
Mean Rhone discharge 1170 m<sup>3</sup>/s



Scenario 6: "Orsure" scenario  
Mean wind speed : 17 km/h  
Mean Rhone discharge 2016 m<sup>3</sup>/s



852



853

854

855 *Fig 7 : Radioactive surface plume shape in the GoL under the most representatives*  
 856 *temporal windows of the 6 scenarios for a released activity of 1TBq of <sup>137</sup>Cs in 48*  
 857 *hours. Wind orientation is shown by the yellow arrows.*

858

859

860

861

862

863

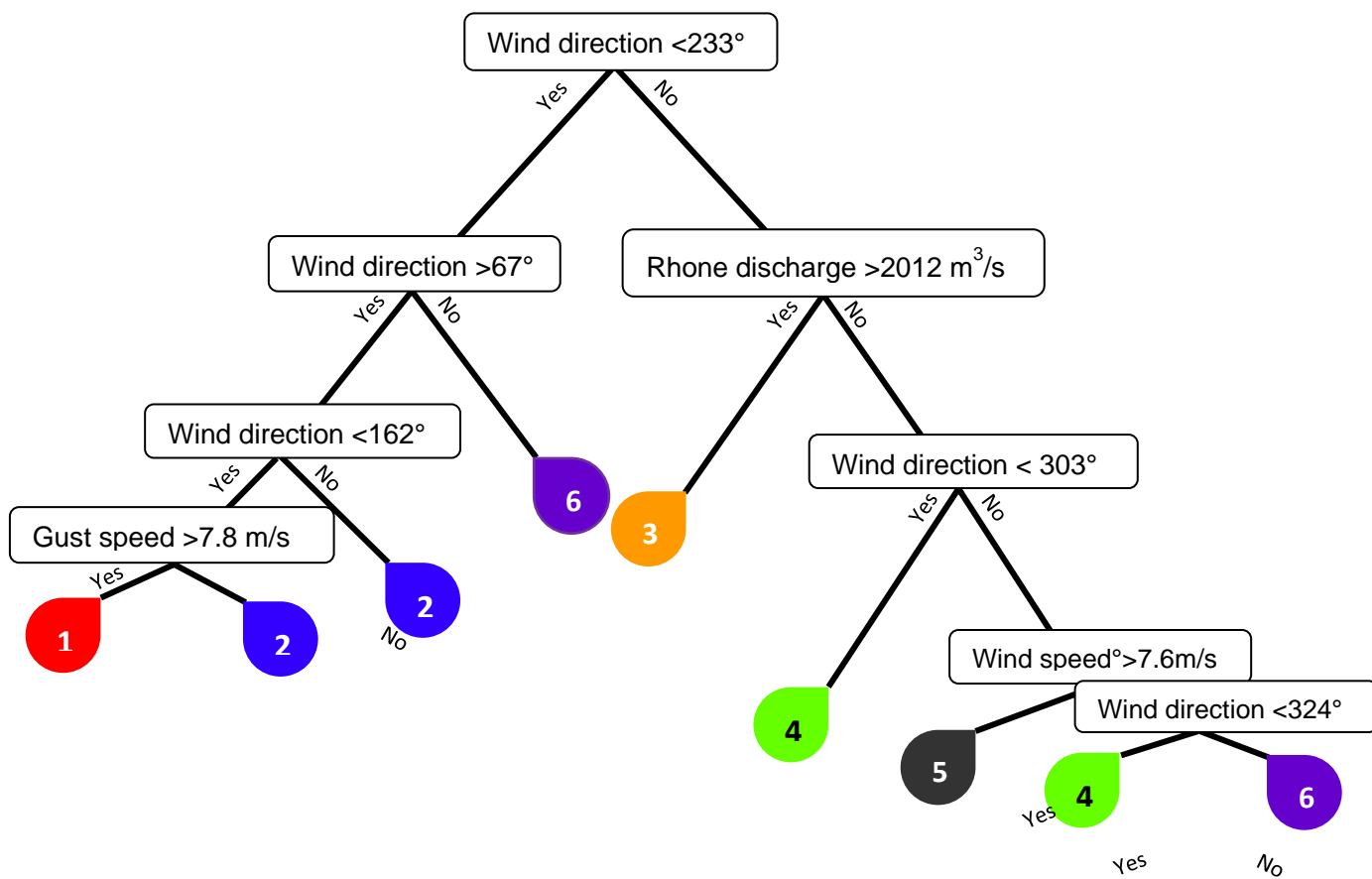
864

865

866

867

868



869

870

871

872

873

874

875

*Fig 8 : Simplified decision tree for scenario identification*

876

877

878

879

880

881

882

883

884

885

886